



Article

Magnetic Ion Imprinted Polymers (MIIPs) for Selective Extraction and Preconcentration of Sb(III) from Environmental Matrices

Silindokuhle Jakavula^{1,2}, Nkositatile Raphael Biata^{1,2}, Kogobi M. Dimpe¹, Vusumzi Emmanuel Pakade³ 
and Philiswa Nosizo Nomngongo^{1,2,*} 

¹ Department of Chemical Sciences, Doornfontein Campus, University of Johannesburg, Doornfontein 2028, South Africa; jakavulasilindokuhle@yahoo.com (S.J.); raphaelbiata@gmail.com (N.R.B.); mdimpe@uj.ac.za (K.M.D.)

² Department of Science and Innovation-National Research Foundation South African Research Chair Initiative (DSI-NRF SARCHI), Nanotechnology for Water, University of Johannesburg, Doornfontein 2028, South Africa

³ Department of Chemistry, Vaal University of Technology, Private Bag X 021, Vanderbijlpark 1911, South Africa; vusumzip@vut.ac.za

* Correspondence: pnnomngongo@uj.ac.za

Abstract: Antimony(III) is a rare element whose chemical and toxicological properties bear a resemblance to those of arsenic. As a result, the presence of Sb(III) in water might have adverse effects on human health and aquatic life. However, Sb(III) exists at very ultra-trace levels which may be difficult for direct quantification. Therefore, there is a need to develop efficient and reliable selective extraction and preconcentration of Sb(III) in water systems. Herein, a selective extraction and preconcentration of trace Sb(III) from environmental samples was achieved using ultrasound assisted magnetic solid-phase extraction (UA-MSPE) based on magnetic Sb(III) ion imprinted polymer-Fe₃O₄@SiO₂@CNFs nanocomposite as an adsorbent. The amount of antimony in samples was determined using inductively coupled plasma optical emission spectrometry (ICP-OES). The UA-MSPE conditions were investigated using fractional factorial design and response surface methodology based on central composite design. The Sb(III)-IIP sorbent displayed excellent selectivity towards Sb(III) as compared to NIIP adsorbent. Under optimised conditions, the enrichment factor, limit of detection (LOD) and limit of quantification (LOQ) of UA-MSPE/ICP-OES for Sb(III) were 71.3, 0.13 µg L⁻¹ and 0.44 µg L⁻¹, respectively. The intra-day and inter-day precision expressed as relative standard deviations (%RSDs, n = 10 and n = 5) were 2.4 and 4.7, respectively. The proposed analytical method was applied in the determination of trace Sb(III) in environmental samples. Furthermore, the accuracy of the method was evaluated using spiked recovery experiments and the percentage recoveries ranged from 95–98.3%.

Keywords: ion imprinted polymers; antimony(III); magnetic solid-phase extraction; environment matrices; Sb(III) IIP@Fe₃O₄@CNF@SiO₂



Citation: Jakavula, S.; Biata, N.R.; Dimpe, K.M.; Pakade, V.E.; Nomngongo, P.N. Magnetic Ion Imprinted Polymers (MIIPs) for Selective Extraction and Preconcentration of Sb(III) from Environmental Matrices. *Polymers* **2022**, *14*, 21. <https://doi.org/10.3390/polym14010021>

Academic Editor: Beom Soo Kim

Received: 1 December 2021

Accepted: 15 December 2021

Published: 22 December 2021

Publisher's Note: MDPI stays neutral with regard to jurisdictional claims in published maps and institutional affiliations.



Copyright: © 2021 by the authors. Licensee MDPI, Basel, Switzerland. This article is an open access article distributed under the terms and conditions of the Creative Commons Attribution (CC BY) license (<https://creativecommons.org/licenses/by/4.0/>).

1. Introduction

Antimony (Sb) is a toxic metalloid that exists at very ultra-trace levels in the environment [1–3]. Inorganic compounds of Sb are said to be more toxic than other metal compounds [4]. Human beings may be exposed to Sb by breathing air, drinking water and eating food that is contaminated with Sb [5]. The toxicity of Sb depends on its chemical species. For instance, Sb(III) is ten times more toxic than Sb (V) [6] and Sb(III) shows high affinity towards red blood cells [5]. Antimony levels in the environment have been elevated due to its rapid use in batteries, plastics, paints, alloys and semiconductors [7]. In addition, Sb is used as a catalyst in the production of poly(ethylene terephthalate) (PET), which is used in plastic bottles [8]. These PET bottles are used as packages for beverages

and water [9,10]. As such, Sb is often detected in bottled water and beverages because of leakage from PET through storage [11,12].

Due to the toxicity of Sb, there are numerous analytical techniques that have been used for the determination of total and Sb species. These include inductively coupled plasma mass spectrometry (ICP-MS) [13], graphite furnace atomic absorption spectrometry (GF-AAS) [14] and inductively coupled plasma optical emission spectrometry (ICP-OES) [15], etc. Due to low concentrations of Sb and complexity of sample matrices, sample preparation is required prior to its determination [16]. Several researchers have developed various sample preparation methods, which include solid phase extraction (SPE) [2], ultrasound-assisted cloud point extraction (UA-CPE) [17], dispersive micro-solid phase extraction (DSPME) [18] and magnetic solid phase extraction (MSPE) [15], among others.

Among these methods, solid phase-based procedures have attracted a lot of attention. This is due to their attractive features such as flexibility, simplicity and choice of adsorbent. Therefore, in order to successfully and selectively extract Sb in various matrices, the choice of suitable adsorbent is required [19]. As a result, several sorbents have been used for extraction and preconcentration of Sb. These include Mg-Fe-OH- layered double hydroxide [20], zirconium oxide-carbon nanofibres [21], reduced graphene oxides/ Mn_3O_4 [22], magnetic nickel ferrite (NiFe_2O_4) nanoparticles [23] and ion imprinted polymers (IIPs) [19], to name a few. Ion imprinted polymers are one of the promising sorbents that have been developed for selective extraction and preconcentration of trace metal ions [24,25].

Over the past years, IIPs have attracted attention for the determination, speciation and removal of metal ions due to their advantages, such as simplicity, high adsorption capacity, high selectivity, low costs, reusability and high extraction efficiency [26]. The general procedure for the synthesis of IIPs involves the formation of a metal ion (template) complex with a suitable ligand followed by copolymerisation in the presence of cross-linker, initiator and a monomer where a polymer matrix with recognition sites is formed [27]. Various researchers have reported they explored the use of IIPs as adsorbents for the removal and speciation of toxic trace metals, such as Hg(II) [28], Pb(II) [29], Co(II) [30], Pb(II) [31], As(III) [32], Sb(III) [19,26] and Cd(II) [33], among others. In addition, there are also reports on the use of novel molecular imprinted electrochemical sensor for the detection of different pollutants [34–38]. These studies have shown that the combination of molecularly imprinted polymer (MIP) or IIP with other nanomaterials, such as carbon materials, has attracted great consideration due to the synergetic effect which enables a high mass transfer rate [34–36,38]. In addition, these nanomaterials serve as excellent substrate in surface imprinting processes and some of these materials (e.g., magnetic nanoparticles) provide better separability and reusability. According to the literature search, when compared to other toxic trace metals, few studies have explored the use of IIPs for selective extraction, preconcentration or removal of Sb [6,19,27,39–42]. Notwithstanding the fact that there are already existing reports on the application of IIPs for the analysis of Sb in water, there is a need for continuously monitoring the amount of Sb in these matrices.

Therefore, the aim of this study was to prepare Sb(III)-IIP by surface imprinting technique, using styrene as a monomer and $\text{Fe}_3\text{O}_4@\text{CNFs}@Si\text{O}_2$ nanocomposite as a supporting substrate. Carbon nanofibres were chosen because of their attractive properties, such as large surface area, strong interaction with various substances as well as high affinity towards metals. However, the major drawback of using CNFs as support for IIPs is separability and regeneration. Therefore, anchoring of magnetic nanomaterials in CNFs matrix allows better separation and reusability. Lastly, incorporating mesoporous silica to magnetic CNFs leads to an excellent IIP carrier with large surface areas and tuneable pore sizes. The Sb(III)-IIP- $\text{Fe}_3\text{O}_4@\text{CNFs}@Si\text{O}_2$ was characterised using X-ray diffraction (XRD), Fourier-transform infrared spectroscopy (FTIR), scanning electron microscopy (SEM), energy dispersive X-ray spectroscopy (EDS) and transmission electron microscopy (TEM). The prepared Sb(III)-IIP- $\text{Fe}_3\text{O}_4@\text{CNFs}@Si\text{O}_2$ was used as adsorbent for selective extraction and preconcentration of Sb(III) in surface water samples prior to ICP-OES analysis. Factors affecting the preconcentration process were optimised using a multivariate approach.

2. Materials and Methods

2.1. Reagents and Materials

Analytical grade chemicals and ultrapure water were employed during the experiments. Antimony single standard (1000 mg L^{-1}), ammonium pyrrolidine dithiocarbamate (APDC), iron (II) chloride tetrahydrate, carbon nanofibres (CNFs), hydrochloric acid, iron (III) chloride hexahydrate, ethanol, ammonia (25%), tetraethyl orthosilicate (TEOS), ethanol, 2-methoxy ethanol, antimony(III) chloride, styrene, ethylene glycol dimethacrylate (EGDMA), chloroform, 1,1'-azobisisobutyronitrile (AIBN) and nitric acid (65%) were obtained from Sigma-Aldrich (St. Louis, MO, USA).

2.2. Synthesis of Fe_3O_4 Coated with CNFs

The synthesis of Fe_3O_4 coated with CNFs was conducted according to previous studies [43]. To describe the method briefly, appropriate amounts of FeCl_2 (2.50 g) and FeCl_3 (6.82 g) were dissolved in deionised water and 2 mL of HCl was added in the mixture to facilitate the complete dissolution of the iron salts. About 2.5 g of CNFs were dispersed in the solution prepared above under continuous stirring. To precipitate the final product, about 250 mL of $1.5 \text{ mol L}^{-1} \text{ NH}_3$ was added (dropwise) to the mixture until the pH of the solution ranged from 11–12. The mixture was placed on a heater stirrer and the temperature was set at 80–90 °C. The mixture was stirred until the resultant black product has formed. The mixture was cooled to ambient temperature and the Fe_3O_4 @CNFs nanocomposite was collected using external magnet. The Fe_3O_4 @CNFs nanocomposite was washed with ethanol–water (50:50) mixture and dried at 100 °C for 2 h.

2.3. Synthesis of Fe_3O_4 @CNFs@ SiO_2 and Sb(III)-IIP- Fe_3O_4 @ SiO_2 @CNFs Nanocomposites

Synthesis of the Fe_3O_4 @CNFs@ SiO_2 nanocomposite was carried according to previous studies with minor adjustments [33]. Firstly, Fe_3O_4 @CNFs (2.0 g) was dispersed in alcoholic aqueous solution (45 mL of H_2O and 100 mL of ethanol). The mixture was heated at 70 °C and 4.5 mL of ammonium solution (25 wt. %) was added while stirring. The mixture was further stirred continuously for 15 min. Ethanolic solution (50 mL) containing TEOS (8.25% *v/v*) was added dropwise for 90 min and the mixture was stirred at 70 °C continuously for 6 h. The final product was separated from the supernatant using external magnet. The Fe_3O_4 @CNFs@ SiO_2 nanocomposite was subsequently washed with ethanol (to remove unreacted TEOS) followed by rinsing with distilled water and dried at 60 °C in an oven for 12 h. The synthesis of Sb(III)-IIP was conducted according to [44] and the detailed procedure is presented in Supplementary Information.

2.4. Ultrasonic-Assisted Magnetic Solid Phase Extraction (UA-MSPE) Procedure

The UA-MSPE method was performed according to [45]. The extraction procedure was conducted as follows: 10–100 mg of Sb(III)-IIP- Fe_3O_4 @ SiO_2 @CNFs adsorbent was placed in a centrifuge tube followed by the addition of 10 mL of sample solution at pH = 2, pH = 5.5, pH = 9. The extraction and preconcentration steps were achieved by the dispersion of the adsorbent in the sample via ultrasonication for 5–30 min. The adsorbent containing the adsorbed analyte was separated from the aqueous solution by application of an external magnet at the base of the centrifuge tube. The supernatant was filtered using 0.22 μm PVDF membrane and the filtrate was analysed using inductively coupled plasma-optical emission spectrometer (ICP-OES) (iCAP 6500 Duo, Thermo Scientific, Hemel Hempstead, UK). The ICP-OES conditions are stated in Table S1.

2.5. Optimisation Strategy

The 2^{6-2} fractional factorial design (FrFD) was used for the screening of the most influential experimental factors affecting the extraction and preconcentration procedure. These include elution time (ET), sample pH, eluent volume (EV), eluent concentration (EC), sonication time (ST) and mass of adsorbent (MA). The independent and their levels are shown in Table 1.

Table 1. Lower and higher levels as well as central points of the investigated independent variables.

Parameters	Lower Level (–)	Central Point (0)	Higher Level (+)
Adsorbent Mass (mg)	20	35	50
Elution time (min)	5	17.5	30
Eluent volume (mL)	7	8.5	10
Eluent concentration (M)	1	3	5
Sonication time (min)	5	22.5	40
pH	2	5.5	9

After the screening process using FrFD, the most influential parameters were found to be MA and pH. These factors were optimised using response surface methodology (RSM) based on central composite design (CCD).

2.6. Adsorption Experiments

The adsorption equilibrium experiments were carried out under optimised conditions. Briefly, 56 mg of Sb(III)-IIP-Fe₃O₄@SiO₂@CNFs and IIP-Fe₃O₄@SiO₂@CNFs were added into 30.0 mL of a synthetic sample that contains Sb(III) at initial concentrations ranging from 2–10 mg/L. The samples were sonicated for 10 min at 25 °C and followed by external magnet separation. The supernatant was filtered and analysed for residual Sb(III) using ICP-OES. The amount of Sb(III) in the synthetic samples before adsorption and procedure blanks were determined using ICP-OES. The analytical results obtained were processed using Equation (1) to estimate adsorption capacity (q_e , mg/g).

$$q_e = \frac{(C_0 - C_e)V}{m} \quad (1)$$

where C_0 and C_e are initial and equilibrium concentrations (mg/L) of Sb(III), V is the volume of the sample (L) and m is the mass of the adsorbent (g).

2.7. Selectivity Experiments

The selectivity studies were performed by placing 56 mg of Sb-IIP and NIP into 100 mL sample bottle containing 30 mL of the sample containing Sb(III), Al(III), Cd(II), Cu(II), Sn(IV) and Zn(II) at 10 mg/L (pH = 3). The samples were agitated using ultrasonic bath for 10 min at 25 °C. The remaining concentrations of Al(III), Cd(II), Cu(II), Sb(III), Sn(IV) and Zn(II) were determined using ICP-OES. Parameters such as distribution ratio (D), selectivity coefficient and relative selectivity coefficient were calculated according to Reference [20].

3. Results and Discussion

3.1. Characterisation

3.1.1. X-ray Powder Diffraction (XRD)

A PANalytical X'Pert Pro X-ray diffraction (XRD, PANalytical, Almelo, The Netherlands) was used to assess the crystalline structure of materials. Figure 1 displays the XRD patterns for Fe₃O₄@CNFs, Fe₃O₄@SiO₂@CNF, Sb(III) IIP-Fe₃O₄@SiO₂@CNFs and NIP-Fe₃O₄@SiO₂@CNF. Figure 1a,b displays peaks at 2θ values of 26.5°, 30.4°, 32.7°, 43.3°, 53.8°, 57.2° and 62.9°, which are ascribed to Fe₃O₄ nanoparticle, confirming successful synthesis and incorporation of the magnetic nanoparticles. Figure 1c,d shows the diffractograms for Sb(III) IIP-Fe₃O₄@SiO₂@CNFs and NIP-Fe₃O₄@SiO₂@CNF and the peaks for the magnetic composite were observed at 2θ values of 26.4, 30.3°, 35.8°, 43.2°, 54.0°, 57.2° and 63.0° with reduced intensity. These results confirmed the loss of magnetic nanoparticles during the polymerisation process.

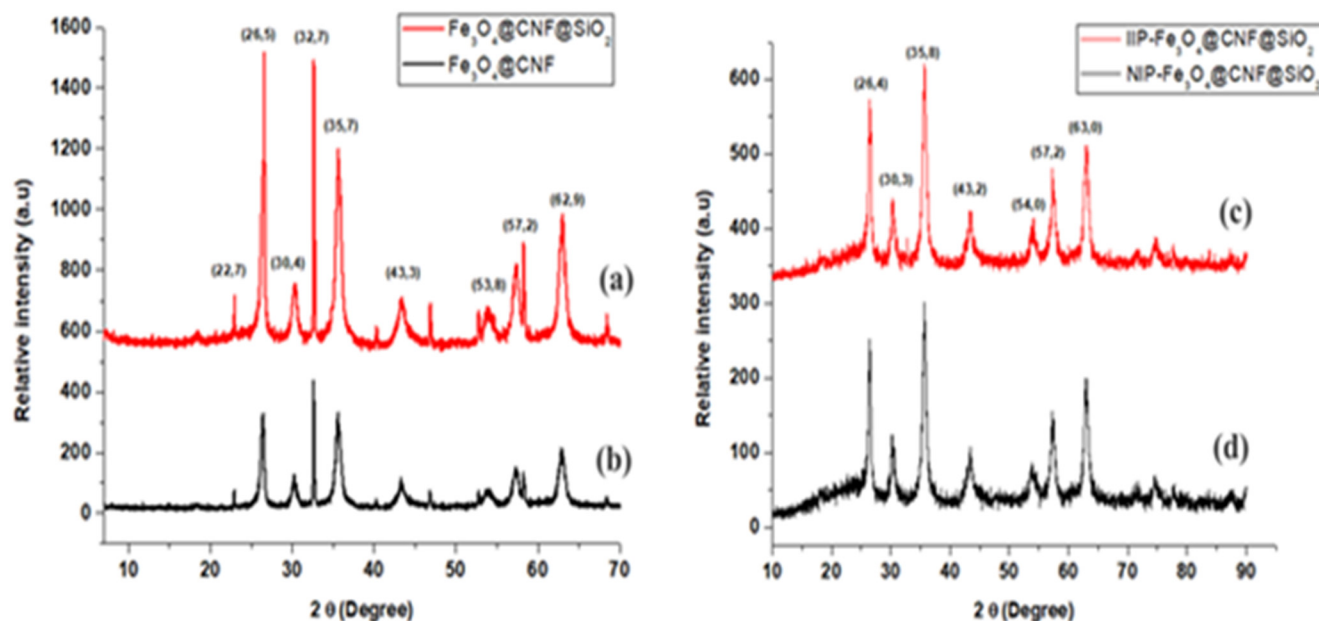


Figure 1. XRD patterns of (a) Fe_3O_4 @CNFs, (b) Fe_3O_4 @ SiO_2 @CNFs, (c) IIP- Fe_3O_4 @ SiO_2 @CNFs and (d) NIP- Fe_3O_4 @ SiO_2 @CNFs.

3.1.2. Fourier-Transform Infrared Spectroscopy (FTIR)

The structural properties of the prepared material were investigated using Perkin Elmer spectrum 100 Fourier-transform infrared spectrometer (FTIR, Waltham, MA, USA). (Figure 2). Figure 2a shows the spectrum of Fe_3O_4 @CNFs and the peak at 604.5 cm^{-1} was assigned to the absorption of the Fe–O bond in Fe_3O_4 . The peak at 1626 cm^{-1} was assigned to the C–C stretching associated with the nanofibre surface defects [46]. The peak at 3142 cm^{-1} was assigned to the –OH stretching of the CNFs. Figure 2b showed new peaks at 756.4 and 1117 cm^{-1} , which were assigned to Si–O vibration and bending vibration of the Si–O–Si bond [47]. These findings confirmed the incorporation of SiO_2 in nanocomposite matrix. Figure 2c,d exhibited characteristic bands of the polymeric matrix showing the presence of styrene–EGDMA polymers in the sample [48]. The peaks observed for the IIP- Fe_3O_4 @ SiO_2 @CNFs and NIP- Fe_3O_4 @ SiO_2 @CNFs were: 2923.17 cm^{-1} aliphatic C–H; 1716.20 cm^{-1} for C=O; and 1157.40 and 1153.89 cm^{-1} for C–O, which is assigned to the EDGMA ester group [48]. In Figure 2c, the C–S band of the APDC shifted from 595.99 (free APDC, Figure 2d) to 632.40 cm^{-1} in IIP, which indicated the formation of complex between Sb(III) and APDC [44].

3.1.3. Scanning Electron Microscope/Energy Dispersive X-ray Spectroscopy (SEM/EDS)

The morphological properties and elemental composition of the synthesised materials were investigated using scanning electron microscopy (SEM, TESCAN VEGA 3 XMU, LMH instrument, Tescan Company, Brno, Czech Republic) coupled with energy dispersive X-ray spectroscopy (EDS). Figure 3 presents the SEM images and respective EDS spectra for (a) Fe_3O_4 @ SiO_2 @CNFs, (b) NIP- Fe_3O_4 @ SiO_2 @CNFs and (c) Sb(III) IIP- Fe_3O_4 @ SiO_2 @CNFs. The SEM/EDS was used to confirm the morphological elemental changes of the nanocomposites. Figure 3a confirmed the incorporation of magnetic nanoparticles on the surface of the carbon nanofibres. Moreover, the elemental analysis results of Fe_3O_4 @ SiO_2 @CNFs nanocomposite confirmed the presence of expected elements including C, O, Si and Fe in the ternary nanocomposite. Figure 3b,c reveals the growth of IIP on the surface of Fe_3O_4 @ SiO_2 @CNFs nanocomposite. In addition, the presence of C, Fe, O, Si and S in Figure 3b confirms that the surface imprinting was successful. Furthermore, the presence of Sb in Figure 3c confirm that the Sb(III) IIP- Fe_3O_4 @ SiO_2 @CNFs was successfully synthesised. The presence of Cl was from antimony chloride which was used during the synthesis of IIP.

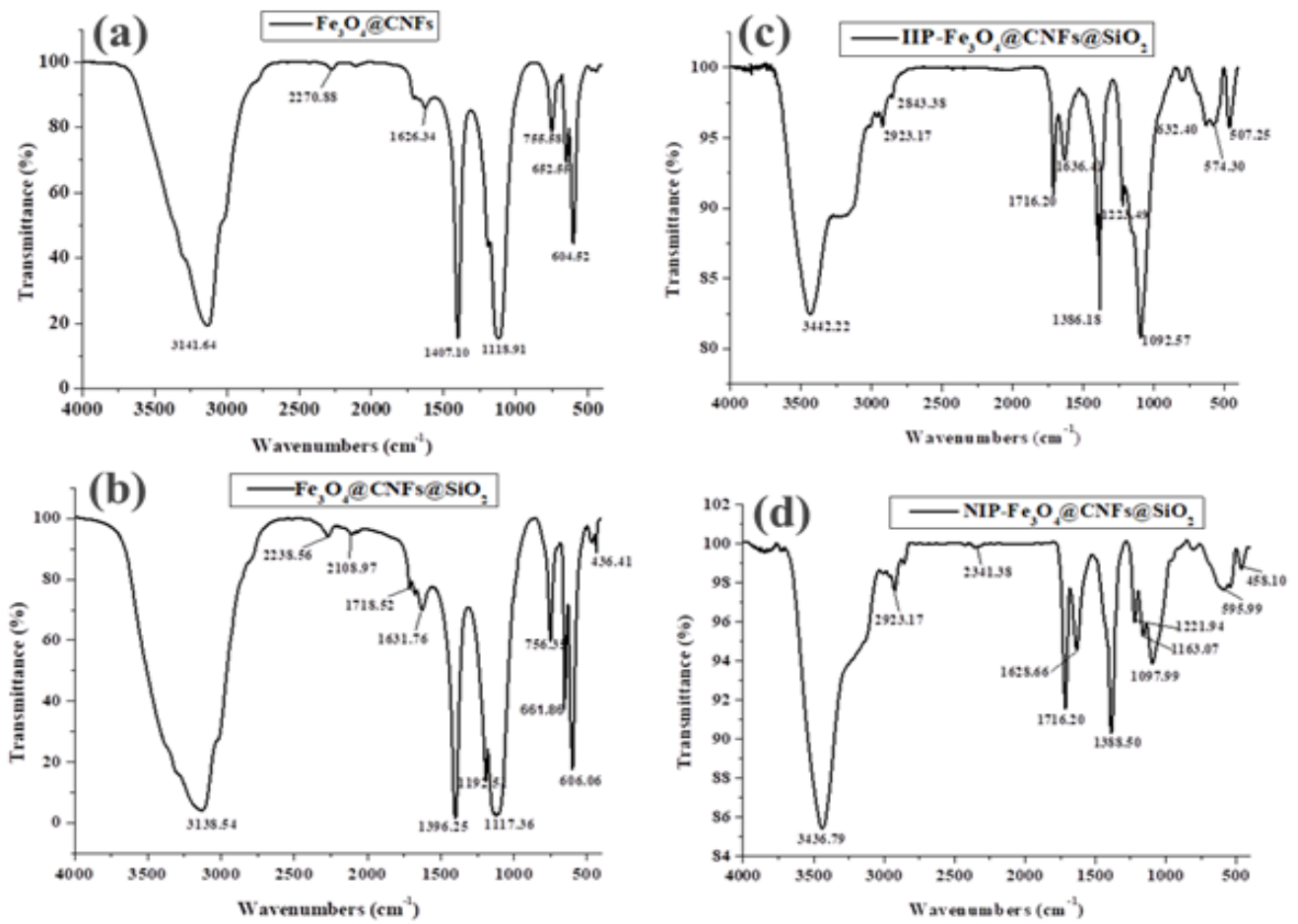


Figure 2. FTIR spectra of (a) $\text{Fe}_3\text{O}_4@\text{CNFs}$, (b) $\text{Fe}_3\text{O}_4@\text{SiO}_2@\text{CNFs}$, (c) $\text{IIP-Fe}_3\text{O}_4@\text{SiO}_2@\text{CNFs}$ and (d) $\text{NIP-Fe}_3\text{O}_4@\text{SiO}_2@\text{CNFs}$.

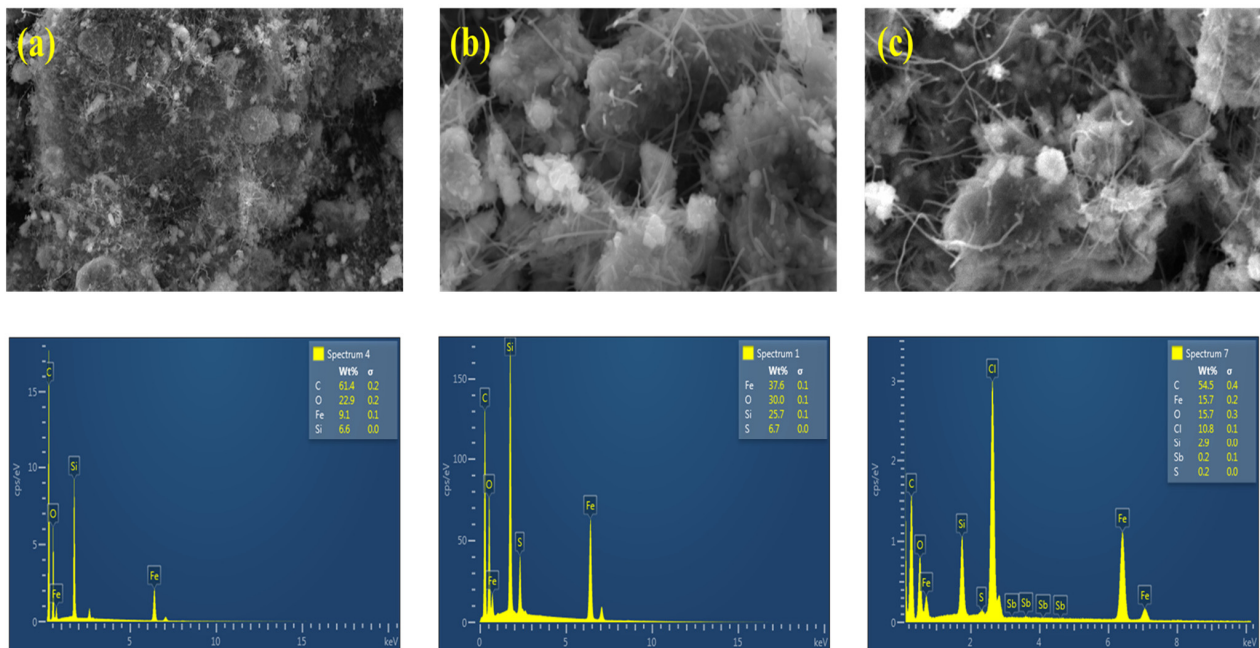


Figure 3. SEM and EDX images of (a) $\text{Fe}_3\text{O}_4@\text{SiO}_2@\text{CNFs}$, (b) $\text{NIP-Fe}_3\text{O}_4@\text{SiO}_2@\text{CNFs}$ and (c) $\text{Sb(III) IIP-Fe}_3\text{O}_4@\text{SiO}_2@\text{CNFs}$.

3.1.4. Transmission Electron Microscopy (TEM)

The transmission electron microscopy (TEM, JEM-2100, JEOL, Tokyo, Japan) was used to investigate the nano structure and particle size of the adsorbents. Figure 4 illustrates the TEM images of (A) $\text{Fe}_3\text{O}_4@\text{SiO}_2@\text{CNFs}$, (B) $\text{NIP-Fe}_3\text{O}_4@\text{SiO}_2@\text{CNFs}$ and (C) $\text{IIP-Fe}_3\text{O}_4@\text{SiO}_2@\text{CNFs}$. Figure 4A reveals that spherical shape of $\text{Fe}_3\text{O}_4@\text{SiO}_2$ nanocomposite evenly dispersed in the surface of carbon nanofibres. Figure 4B,C shows the growth of the polymer on the surface of $\text{Fe}_3\text{O}_4@\text{SiO}_2@\text{CNFs}$ nanocomposite.

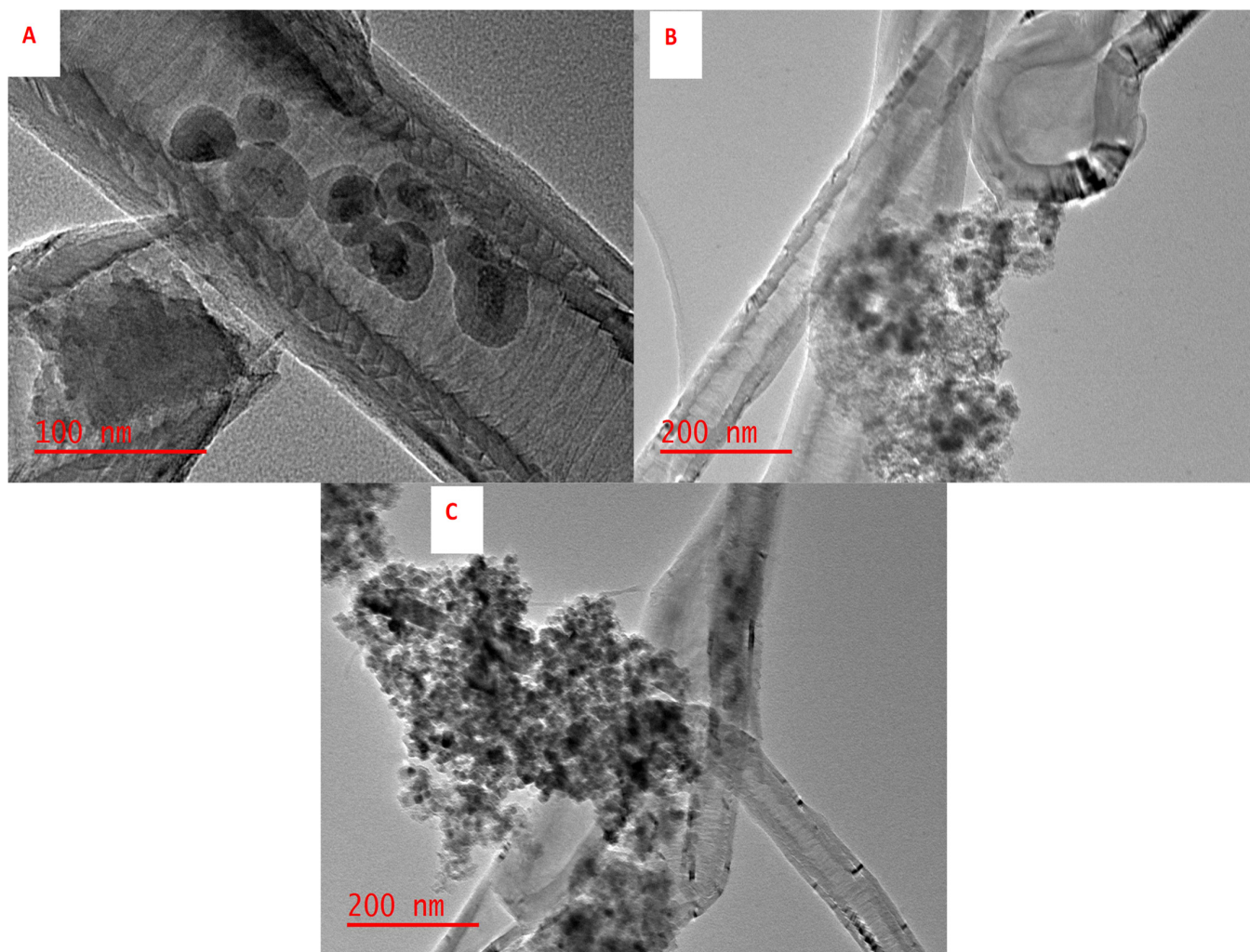


Figure 4. TEM images of (A) $\text{Fe}_3\text{O}_4@\text{SiO}_2@\text{CNFs}$, (B) $\text{NIP-Fe}_3\text{O}_4@\text{SiO}_2@\text{CNFs}$ and (C) $\text{IIP-Fe}_3\text{O}_4@\text{SiO}_2@\text{CNFs}$.

3.2. Optimisation Strategy

The fractional factorial design 2^{6-2} (FrFD) was used for selection of the most influential experimental parameters (eluent concentration (EC), sonication time (ST), elution time (ET), eluent volume (EV), mass of adsorbent (MA) and sample pH). The design matrix and the analytical response are presented in Table S2. The data was processed using Statistica version 13 software. The analysis of variance (ANOVA) was used to examine the significance of each independent factors. ANOVA results presented as Pareto chart (Figure 5) was used to assess the importance of independent variables and their interactions [49]. The results obtained on the Pareto chart showed that MA and pH were significant at 95% confidence level. This means that the two independent variables played a significant role in the preconcentration of Sb(III). Therefore, further optimisation was required to give optimum conditions for MA and pH.

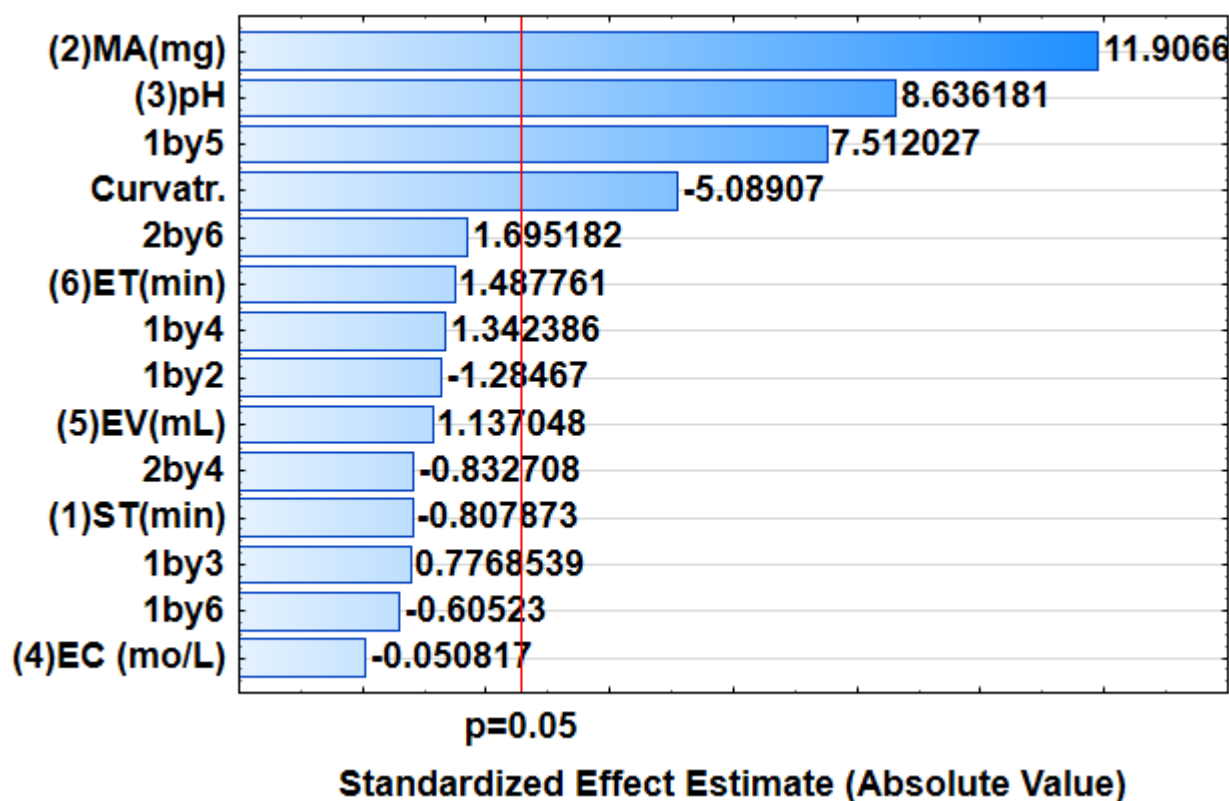


Figure 5. Pareto chart of the standardised effects for the extraction and preconcentration of Sb(III).

3.2.1. Response Surface Methodology

For further optimisation, response surface methodology (RSM) based on central composite design (CCD) was used to evaluate the interaction between MA and pH. The CCD matrix and respective analytical response are shown in Table S3. The 3D response surface plot shows the analytical response against individual factors (Figure 6). As can be seen in Figure 6, an enhanced analytical response (% recovery) at a pH value between 2 and 4 was observed and, for the MA, maximum recoveries were achieved at a mass between 50 and 60 mg. Above pH 4, lower recoveries were observed, and this might be due to the reduced interactions between the negatively charged analyte and positively charged adsorbent.

3.2.2. Estimation of Optimum Conditions Using Desirability Functions

In Figure 7, the desirability functions of 0.0, 0.5 and 1.0 were assigned to undesirable (33.7%), middle (66.5%) and desirable (maximum recoveries, 99.3%), respectively. Herein, the desirability score of 1.0 was chosen to estimate the desirable optimal parameters. Therefore, based on the screening results and desirability score of 1.0, the optimum conditions, were, 3.0, 56 mg, 3.0 mol L⁻¹, 10 min, 20 min and 7.0 mL, for pH, MA, EC, ST, ET and EV, respectively. These conditions were confirmed experimentally (in triplicates) and the experimental recoveries (98.7 ± 1.2%) agreed with the RSM predicted value (99.3%) at 95% confidence level.

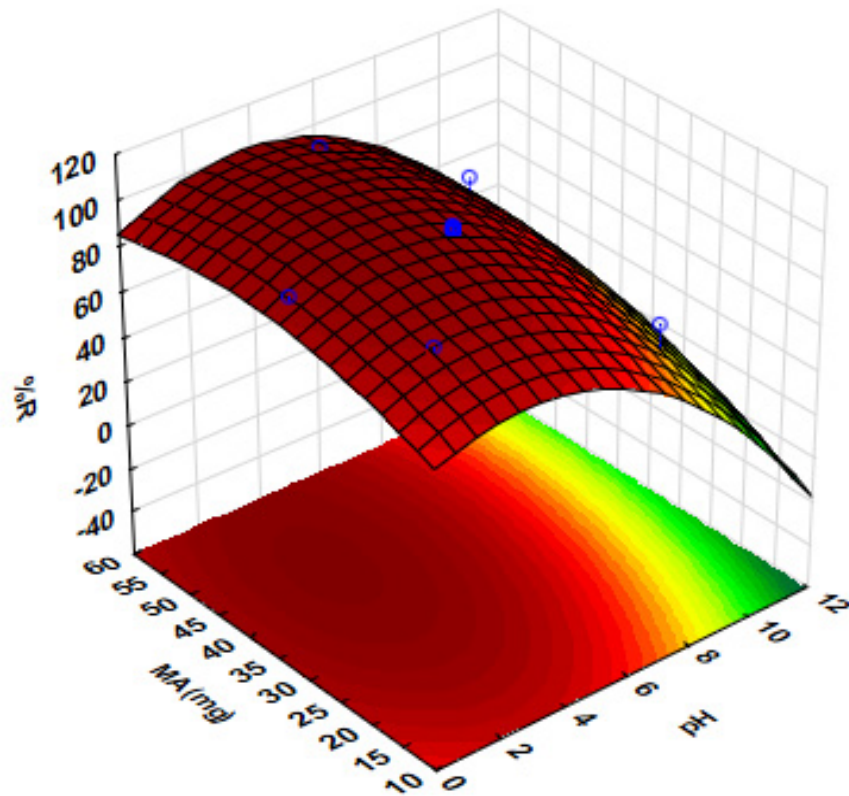


Figure 6. Response surface methodology for the pre-concentration of Sb.

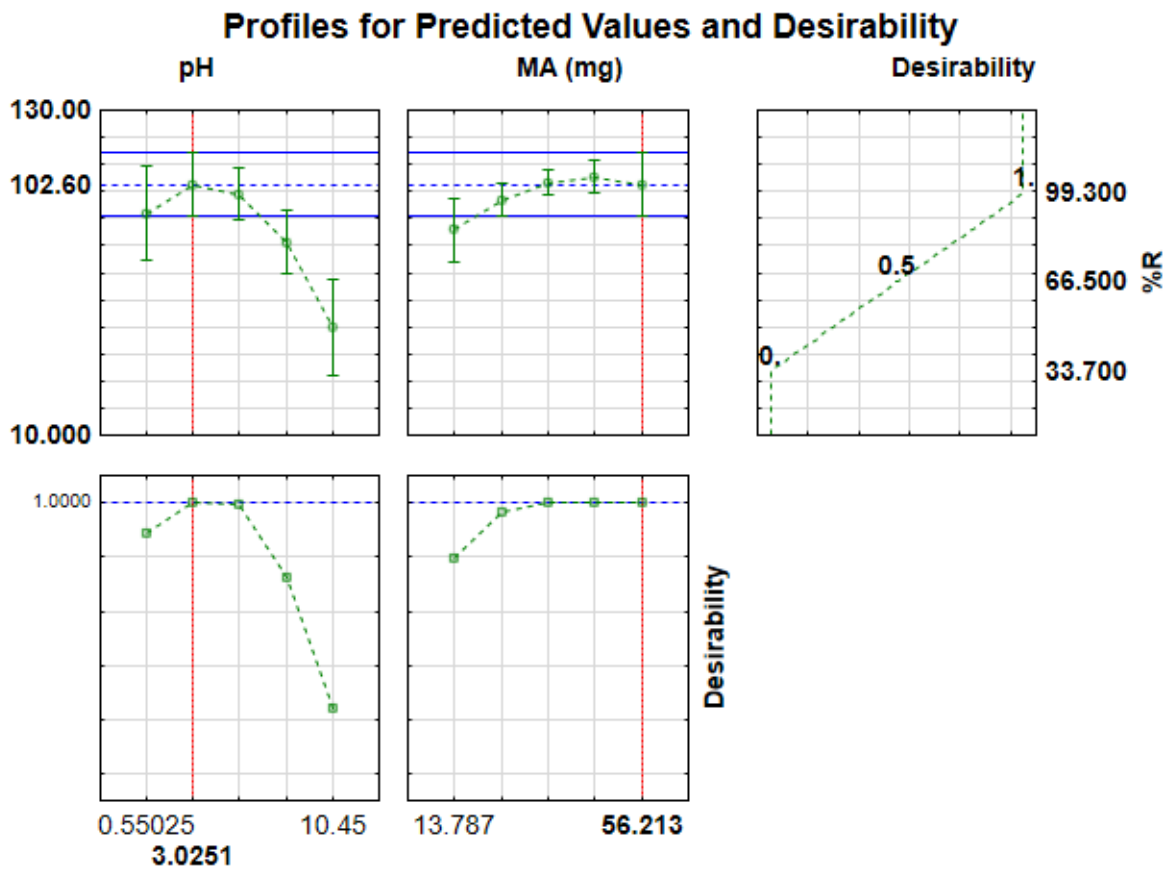


Figure 7. Desirability profile of predicted optimum conditions for the pre-concentration of Sb(III).

3.3. Scatchard Analysis, Adsorption Isotherms and Selectivity Studies

3.3.1. Scatchard Analysis

The theoretical maximum Sb(III) binding or adsorption capacity of IIP was also estimated using Scatchard plot obtained according to Equation (1).

$$\frac{q_e}{C_e} = \frac{q_{max} - q_e}{K_d} \quad (2)$$

where q_e (mg/g) is the adsorption or binding capacity at equilibrium, C_e is the residual concentration of Sb(III) at equilibrium, K_d (mg/L) is the equilibrium dissociation constant at binding sites and q_{max} (mg/g) is the maximum binding [32]. The values of K_d and q_{max} were calculated from the slope and the intercept of the linear plot of q_e/C_e versus q_e [32]. According to the literature, Scatchard plot shape is correlated to the nature of the interaction between the adsorbate and adsorbent [47,50]. For example, if the plot of q_e/C_e versus q_e forms one straight line, this suggests that there is only one type of binding site on the surface of the sorbent [31]. Furthermore, when the Scatchard plot displays an anomaly from linearity (showing two linear plots in one set of data), the results suggest that the adsorbent has more than one type of binding site. These binding sites can be categorised as high-affinity (low K_d value) and low-affinity (high K_d value) binding sites [51,52]. Figure 8 shows the Scatchard plots of Sb(III)-IIP-Fe₃O₄@SiO₂@CNFs and NIP-Fe₃O₄@SiO₂@CNFs. As seen in Figure 8A, the Scatchard plot for Sb(III)-IIP-Fe₃O₄@SiO₂@CNFs was nonlinear and it was divided into two linear sections that had two different slopes. As discussed earlier, these observations suggest that IIP@Fe₃O₄@CNF@SiO₂ had two types of binding sites that have different affinities for the adsorption of Sb(III). On the contrary, the Scatchard plot of NIP-Fe₃O₄@SiO₂@CNFs (Figure 8B) fitted to one linear curve, suggesting that NIP had only one type of binding site.

The slope and intercept of the fitted Scatchard plots were used to estimate the values maximum adsorption capacities and equilibrium dissociation constants for Sb(III)-IIP and NIP (Table 2). The q_{max} and K_d values from the higher affinity binding sites (Curve A-1) were found to be 0.162 13.4 mg/g and mg/L, respectively. In the low affinity binding sites (Curve A-2), the K_d and q_{max} values were 3.03 mg/L and 47.3 mg/g, respectively. Furthermore, the R^2 of curves A-1 and A-2, confirmed existence of two types of binding sites in Sb(III)-IIP and lower R^2 value (0.9215) for Curve A-2 suggested that the cavities in this region were not specific to Sb(III) adsorption. On the other hand, the q_{max} and K_d values for Sb(III)-IIP were 16.1 mg/g and 4.29 mg/L, respectively. As seen in Table 2, the highest dissociation equilibrium constant was obtained when NIP-Fe₃O₄@SiO₂@CNFs was used as an adsorbent. Overall, the trend of dissociation equilibrium constant in this study was as follows: $K_{dA-1} < K_{dA-2} < K_{dB}$. These findings further demonstrate that IIP-Fe₃O₄@SiO₂@CNFs had a higher affinity for Sb(III) than the NIP. Similar results have been reported in the literature [50–52].

Table 2. Scatchard plot parameters.

	Sb(III)-IIP	NIP
Regression equation	$q_e/C_e = -6.1852x + 82.7$ (Curve A-1)	$q_e/C_e = -0.2333 + 3.7493$
R^2	0.9981	0.9557
K_d (mg/L)	0.162	4.29
q_{max} (mg/g)	13.4	16.1
Regression equation (Curve A-2)	$q_e/C_e = -0.2282x + 15.04$	
R^2	0.9215	
K_d (mg/L)	3.05	
q_{max} (mg/g)	47.3	

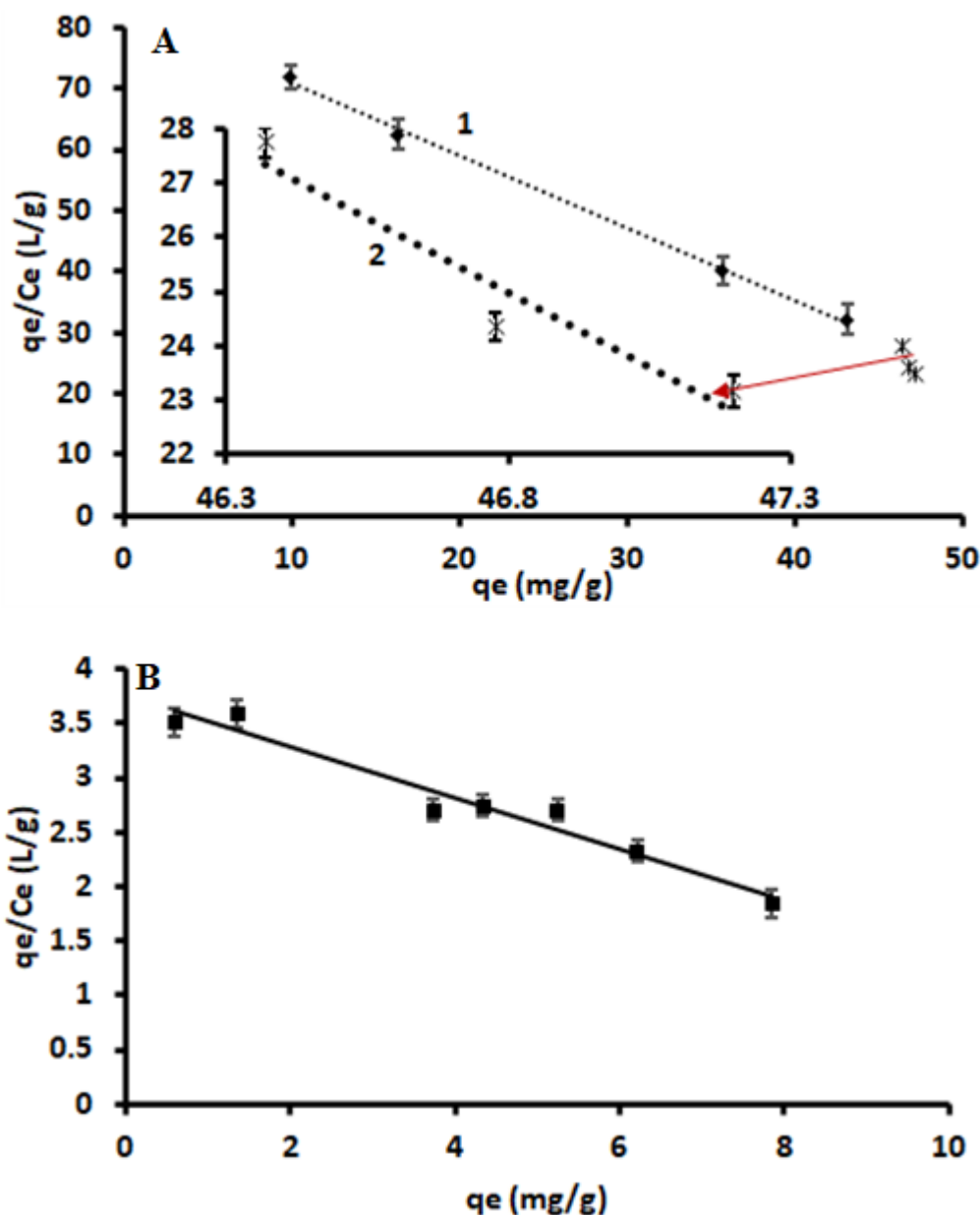


Figure 8. Scatchard plots of (A) Sb(III)-IIP-Fe₃O₄@SiO₂@CNFs and (B) NIP-Fe₃O₄@SiO₂@CNFs.

3.3.2. Adsorption Isotherms

The adsorption of Sb(III) on IIP-Fe₃O₄@SiO₂@CNFs and NIP-Fe₃O₄@SiO₂@CNFs is shown in Figure 9. The Sb(III) adsorption or binding capacity of both IIP-Fe₃O₄@SiO₂@CNFs and NIP-Fe₃O₄@SiO₂@CNFs increased with increasing initial concentration until the saturation point was achieved. The adsorption capacity of IIP-Fe₃O₄@SiO₂@CNFs was found to be higher than that of NIP-Fe₃O₄@SiO₂@CNFs, suggesting that the imprinting played a significant role in the formatting of cavities that are specific to Sb(III). Isotherm models such as Langmuir and Freundlich were used to exam the adsorption behaviour of Sb(III)-IIP-Fe₃O₄@SiO₂@CNFs and NIP-Fe₃O₄@SiO₂@CNFs towards Sb(III). The linear equations for the isotherm models and their constant parameters are presented in Table 3. The linear plots for Langmuir (C_e/q_e vs. C_e) and Freundlich ($\ln q_e$ vs. $\ln C_e$) models using IIP and NIP are shown in Figures S1–S4. The isotherm constant values were estimated from the slope and intercept of each plot (Table 3). The correlation of determination (R^2) values was used to select the model that best explains adsorption results. As seen, the data for Sb(III)-IIP were best described by the Langmuir model ($R^2 = 0.9969$) and the q_{max} value was

47.4 mg g⁻¹. Furthermore, the q_{max} obtained from the Langmuir isotherm model was in agreement with the experimental adsorption capacity (46.7 mg g⁻¹). These results suggest that the adsorption process was dominated by a monolayer sorption on homogenous adsorption or binding sites. The R² (0.9806) of the Freundlich model revealed that there was relative correlation, but Langmuir model explains the adsorption data better. Similarly, adsorption data obtained using NIP-Fe₃O₄@SiO₂@CNFs revealed that the Langmuir model (0.9912) fitted the data better than Freundlich model (0.9869). The adsorption capacity obtained in this study was higher than those reported by Zhang et al. [42] (39.6 mg g⁻¹) and Shakerian et al. [44] (6.7 mg g⁻¹) on the application of IIPs for adsorption antimony. The imprinting factor ($\alpha = q_{max}(\text{IIP})/q_{max}(\text{NIP})$) value was found to be 2.82, confirming successful imprinting.

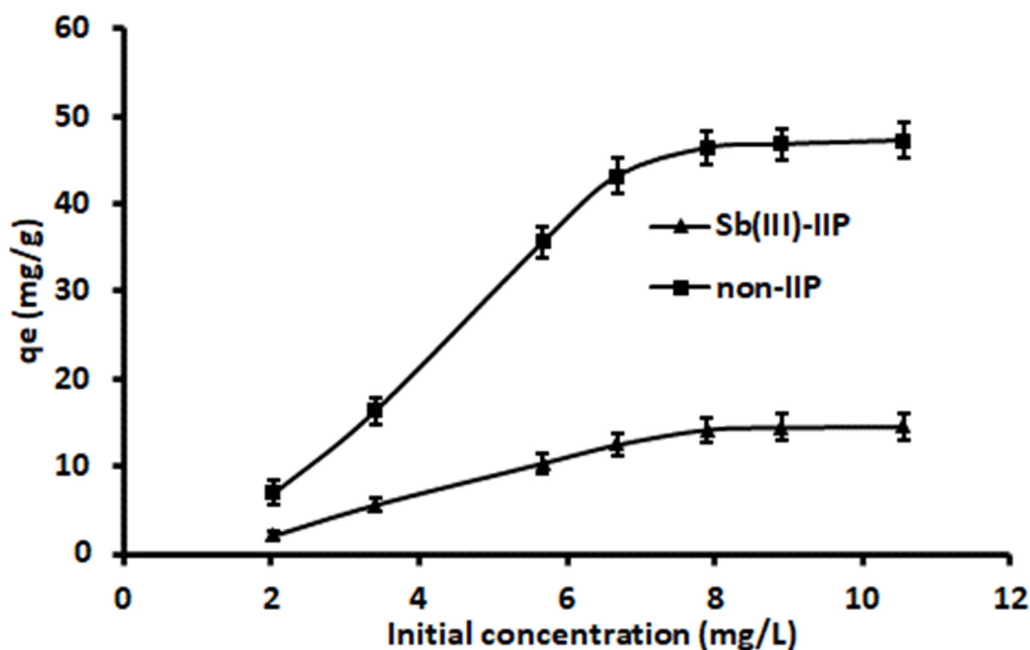


Figure 9. Equilibrium studies for Sb(III) adsorption onto the Sb(III)-IIP-Fe₃O₄@SiO₂@CNFs and NIP-Fe₃O₄@SiO₂@CNFs.

Table 3. Adsorption isotherms models and constant r values.

Isotherms	Parameters	Sb(III)-IIP	Non-IIP
Langmuir $\frac{C_e}{q_e} = \frac{C_e}{q_{max}} + \frac{1}{q_{max}K_L}$	q_{max} (mg/g)	47.4	16.8
	K_L	1.81	0.29
	R ²	0.9969	0.9912
Freundlich $\ln q_e = \ln K_f + \frac{1}{n} C_e$	K_f	33.6	3.74
	n	1.73	1.4
	R ²	0.9806	0.9869

3.3.3. Selectivity

The selectivity studies of Sb(III)-IIP-Fe₃O₄@SiO₂@CNFs and NIP-Fe₃O₄@SiO₂@CNFs were carried out using a multielement sample solution containing Sb(III), Al(III), Cd(II), Cu(II), Sn(IV), Zn(II). Table 4 presents the selectivity experiment data and parameters, such as distribution ratio (D), adsorption capacities (q_e), selectivity coefficient (β), relative selectivity coefficient (β_r) and imprinting factor (α). Table 4 shows that the distribution ratio of Sb(III) ions for the Sb(III)-IIP adsorbent was 10 times higher than that of Sb(III)-NIP. On the contrary, the distribution ratio of co-existing ions for Sb(III)-IIP was somehow lower than or equal to that of NIP except for Sn(IV). Furthermore, the adsorption capacity of Sb(III)-IIP towards Sb(III) was higher than other coexisting ions. Selectivity coefficient

values of Sb(III)-IIP for Sb(III), Al(III), Cd(II), Cu(II), Sn(IV) and Zn(II) were 6–25 times higher than NIP, indicating that the IIP had higher binding specificity for Sb(III). Moreover, the imprinting factor value of the Sb(III) was greater than 1, demonstrating that the Sb(III)-IIP had a higher affinity toward the target analyte. These findings demonstrated that IIP-Fe₃O₄@SiO₂@CNFs had strong binding property towards Sb(III) in the presence of other elements.

Table 4. Selectivity studies.

Metal Ions	q_e (mg/g)		Distribution Ratio (D, mL/g)		β		β_r	α
	IIP	NIP	IIP	NIP	IIP	NIP		
Sb	46.1	16.6	22.2	2.19				2.78
Al	6.52	7.97	0.69	0.87	32.3	2.52	12.8	0.82
Cd	8.41	8.53	0.92	0.94	24.1	2.33	10.3	0.99
Cu	3.70	8.46	0.37	0.93	60.0	2.35	25.5	0.44
Sn	11.2	12.1	2.19	1.44	10.2	1.52	6.67	0.93
Zn	6.24	7.47	0.66	0.80	33.9	2.71	12.5	0.83

3.4. Analytical Performances

The linearity, limit of detection (LOD), limit of quantification (LOQ) and the precision (intra-day and inter-day) were used to evaluate the performance of the method. The linearity was assessed by analysing a series of standard solutions (0–150 $\mu\text{g L}^{-1}$) using the UA-MSPE/ICP-OES method. The linear range was obtained between 0.44 and 100 $\mu\text{g L}^{-1}$ with a correlation of determinations (R^2) of 0.9976. The LOD and LOQ were 0.13 and 0.44 $\mu\text{g L}^{-1}$, respectively. To investigate the precision of the method, a standard solution containing 100 $\mu\text{g L}^{-1}$ Sb(III) ions was analysed repeatedly using the UA-MSPE/ICP-OES method. The intra-day ($n = 10$) and inter-day ($n = 5$ working days) expressed as relative standard deviations (RSD) were 2.4 and 4.7%, respectively. The enrichment factor of the proposed UA-DSPE/ICP-OES procedure was 71.3.

The analytical characteristics of the IIP-Fe₃O₄@SiO₂@CNFs adsorbent were compared with those reported in the literature for the preconcentration of Sb(III) and are presented in Table 5. The developed method showed improved or similar analytical performance in terms of LOD, LOQ and linearity as compared to those reported by References [48–50,52]. However, the current method had high LOD and LOQ as well as narrow linear range as compared to those reported in the literature [2,17,39,51,53]. In addition, the preconcentration factor of the current method was lower than those reported elsewhere [2,17,48].

Table 5. Comparison of the proposed adsorbent with other reported adsorbent for extraction and preconcentration of Sb.

Analyte	Adsorbent	Linear Range ($\mu\text{g L}^{-1}$)	LOD ($\mu\text{g L}^{-1}$)	LOQ ($\mu\text{g L}^{-1}$)	PF	RSD (%)	Refs
Sb	PAN	0.027–650	0.008	0.027	150	1.8–4.1	[17]
Sb(III)	SiO ₂ /Al ₂ O ₃ /SnO ₂	0.50–5.00	0.17	0.56	136	-	[53]
Sb(III)	TAR	0.5–180	0.13	0.43	-	0.9	[54]
Sb	Zr-NPs	30–250	8.0	26.8	-	-	[55]
Sb(III)	IIP	-	0.04	0.13	-	2.3	[42]
Sb, Sb(III)	Mercapto-functionalised hybrid sorbent	-	0.0025	0.008	-	1.6	[56]
Sb(III)	TAC	0.93–180	0.28	0.93	-	3.6	[54]
Sb	IIP	-	0.0039	0.13	-	3.1	[44]
Sb	DBD	1–200	0.2	0.67	-	3	[57]
Sb(III)	POIP	-	0.006	0.02	100	4.2	[2]
Sb	PIL	0.20–200	0.084	0.28	-	<9	[58]
Sb(III)	IIP-Fe ₃ O ₄ @SiO ₂ @CNFs	0.44–100	0.13	0.44	71.3	2.4 and 4.7	This work

IIP: ion imprinted polymers, PIL: polymeric ionic liquid, DBD: dielectric barrier discharge, POIP: polystyrene oleic acid imidazole polymer, TAR: 4-(2-thiazolylazo) resorcinol, TAC: 2-(2-thiazolylazo)-p-cresol, PAN: peroxyacetyl nitrate, Zr-NPs: zirconium nanoparticles, SiO₂/Al₂O₃/SnO₂: silicon dioxide/aluminium oxide/tin oxide.

3.5. Application to Real Samples

The applicability of Sb(III)-IIP-Fe₃O₄@SiO₂@CNFs adsorbent on selective extraction and preconcentration of Sb(III) in real water samples was studied. The method was applied for the analysis of Sb(III) in surface water collected from the local dams (DW1 and DW2) and river (RW). The concentrations of Sb(III) were 88.7, 9.7 and 40.5 µg L⁻¹ in DW1, DW2 and RW, respectively. These results were compared with independent ICP-MS analysis, whereby the samples were analysed directly. The ICP-MS results and the ones obtained using the proposed method agreed at 95% confidence level. Therefore, it can be concluded that the use of Sb(III)-IIP-Fe₃O₄@SiO₂@CNFs as an adsorbent in UA-MSPE resulted in the sensitivity and selectivity determination of Sb(III) in water samples. The concentrations of Sb(III) obtained in our study were compared with global concentrations of antimony in different water samples (Table 6). As seen, the levels of Sb(III) obtained in this study were comparable with those reported elsewhere [50,54,55]. However, they were found to be higher than those reported in Algeria, Mexico and Brazil (Table 6). High levels of Sb in surface water and ground water samples have been reported in China and Turkey (Table 6).

Table 6. Global concentration of Sb in water samples.

Country	Matrix	Concentration of Sb (µg L ⁻¹)	Refs
Mexico	Drinking water	0.28–2.30	[12]
China	Ground water	6–30,000	[59]
Algeria	Drinking water	0.50–1.12	[60]
Pakistan	Drinking water	28	[61]
Brazil	Mineral and surface water	0.26–0.30 and 0.41–1.23	[62]
Brazil	Mineral water	0.54–1.04	[53]
Turkey	Wastewater	300–2000	[63]
China	Surface water	30–150	[64]
Greece	Tap water	10–100	[65]
China	Wastewater	330–11,400	[66]
South Africa	Dam and river water	9.7–88.7	This work

4. Conclusions

In this work, a simple, sensitive and highly selective method based on UA-MSPE/ICP-OES was developed for the analysis of trace amounts of Sb in surface water samples. Sb(III)-IIP-Fe₃O₄@SiO₂@CNFs was used as an adsorbent in UA-MSPE. The SEM, XRD, TEM and EDS confirmed the successful synthesis of the nanocomposite. Parameters affecting the extraction and preconcentration of Sb(III) were optimised using RSM based on CCD. Under optimised conditions, the developed method displayed good analytical performance for extraction, preconcentration and determination of Sb(III) ions in environmental samples. The adsorbent displayed high adsorption capacity (47.8 mg g⁻¹), low LOD (0.13 µg L⁻¹) and high precision (2.4%) when compared to the previous study. Finally, the method was applied for analysis of Sb(III) in real surface water samples and the results agreed with the reference method. These results proved that Sb(III)-IIP-Fe₃O₄@SiO₂@CNFs nanocomposite is the suitable adsorbent for trace analysis of Sb(III).

Supplementary Materials: The following are available online at <https://www.mdpi.com/article/10.3390/polym14010021/s1>, Table S1: Operating parameters of an ICP-OES Table S2: Fractional factorial design matrix and analytical response, Table S3: Central composite design matrix and analytical response, Figure S1: Linearised Langmuir isotherm model for IIP, Figure S2: Linearised Freundlich isotherm model for IIP, Figure S3: Linearised Langmuir isotherm model for NIP, Figure S4: Linearised Freundlich isotherm model for NIP.

Author Contributions: Conceptualization, S.J., K.M.D. and V.E.P.; methodology, S.J. and N.R.B.; software, P.N.N.; validation, S.J. and V.E.P.; formal analysis, S.J. and P.N.N.; resources, P.N.N.; data curation, S.J., N.R.B. and P.N.N.; writing—original draft preparation, S.J.; writing—review and editing, S.J., N.R.B., V.E.P. and P.N.N.; visualization, V.E.P.; supervision, K.M.D., V.E.P. and P.N.N.;

project administration, P.N.N.; funding acquisition, P.N.N. All authors have read and agreed to the published version of the manuscript.

Funding: This research was supported by the National Research Foundation South Africa (DSI-NRF SARChI funding instrument), grant number 91230.

Institutional Review Board Statement: Not applicable.

Informed Consent Statement: Not applicable.

Data Availability Statement: Data are included as the Supplementary Materials and if raw data are required, they will be made available upon request.

Acknowledgments: The authors wish to acknowledge the University of Johannesburg, Faculty of Science and Department of Chemical Sciences for laboratory space.

Conflicts of Interest: The authors have no conflict to declare.

References

1. He, M.; Wang, N.; Long, X.; Zhang, C.; Ma, C.; Zhong, Q.; Wang, A.; Wang, Y.; Pervaiz, A.; Shan, J. Antimony speciation in the environment: Recent advances in understanding the biogeochemical processes and ecological effects. *J. Environ. Sci.* **2018**, *75*, 14–39. [[CrossRef](#)] [[PubMed](#)]
2. Panhwar, A.H.; Tuzen, M.; Hazer, B.; Kazi, T.G. Solid phase microextraction method using a novel polystyrene oleic acid imidazole polymer in micropipette tip of syringe system for speciation and determination of antimony in environmental and food samples. *Talanta* **2018**, *184*, 115–121. [[CrossRef](#)]
3. Frizzarin, R.M.; Portugal, L.A.; Estela, J.M.; Rocha, F.R.P.; Cerdà, V. On-line lab-in-syringe cloud point extraction for the spectrophotometric determination of antimony. *Talanta* **2016**, *148*, 694–699. [[CrossRef](#)] [[PubMed](#)]
4. Govind, P.; Madhuri, S. Heavy metals causing toxicity in animals and fishes. *Res. J. Anim. Vet. Fish. Sci.* **2014**, *2*, 17–23.
5. Dobrowolski, R.; Adamczyk, A.; Otto, M.; Dobrzyńska, J. Determination of antimony in sediments and soils by slurry sampling graphite furnace atomic absorption spectrometry using a permanent chemical modifier. *Spectrochim. Acta Part B At. Spectrosc.* **2011**, *66*, 493–499. [[CrossRef](#)]
6. Fan, H.-T.; Sun, Y.; Tang, Q.; Li, W.-L.; Sun, T. Selective adsorption of antimony (III) from aqueous solution by ion-imprinted organic–inorganic hybrid sorbent: Kinetics, isotherms and thermodynamics. *J. Taiwan Inst. Chem. Eng.* **2014**, *45*, 2640–2648. [[CrossRef](#)]
7. Fang, L.; Zhang, Y.; Lu, B.; Wang, L.; Yao, X.; Ge, T. New two-step extraction method in antimony speciation using HPLC-ICP-MS technique in inhalable particulate matter (PM_{2.5}). *Microchem. J.* **2019**, *146*, 1269–1275. [[CrossRef](#)]
8. Mihucz, V.G.; Zárny, G. Occurrence of antimony and phthalate esters in polyethylene terephthalate bottled drinking water. *Appl. Spectrosc. Rev.* **2016**, *51*, 183–209. [[CrossRef](#)]
9. Biata, N.R.; Nyaba, L.; Ramontja, J.; Mketi, N.; Nomngongo, P.N. Determination of antimony and tin in beverages using inductively coupled plasma-optical emission spectrometry after ultrasound-assisted ionic liquid dispersive liquid-liquid phase microextraction. *Food Chem.* **2017**, *237*, 904–911. [[CrossRef](#)]
10. López-García, I.; Rengevicova, S.; Muñoz-Sandoval, M.J.; Hernández-Córdoba, M. Speciation of very low amounts of antimony in waters using magnetic core-modified silver nanoparticles and electrothermal atomic absorption spectrometry. *Talanta* **2017**, *162*, 309–315. [[CrossRef](#)]
11. Atakan, D.; Durukan, İ.; Bektas, S. Determination of antimony from polyethylene terephthalate in drinking water by solid floating organic drop microextraction and electrothermal atomization atomic absorption spectrometry. *Anal. Lett.* **2016**, *49*, 1066–1078. [[CrossRef](#)]
12. Chapa-Martínez, C.A.; Hinojosa-Reyes, L.; Hernández-Ramírez, A.; Ruiz-Ruiz, E.; Maya-Treviño, L.; Guzmán-Mar, J.L. An evaluation of the migration of antimony from polyethylene terephthalate (PET) plastic used for bottled drinking water. *Sci. Total Environ.* **2016**, *565*, 511–518. [[CrossRef](#)]
13. Amereih, S.; Meisel, T.; Wegsheider, W. Accurate Determination of Total Antimony Using ICP-MS and Optimization Its Extraction Efficiency From Reference and Soil Samples. *Palest. Tech. Univ. Res. J.* **2018**, *6*, 48–58. [[CrossRef](#)]
14. De Jesus, A.; Dessuy, M.B.; Huber, C.S.; Zmozinski, A.V.; Duarte, Á.T.; Vale, M.G.R.; Andrade, J.B. Determination of antimony in pet containers by direct analysis of solid samples using graphite furnace atomic absorption spectrometry and leaching studies. *Microchem. J.* **2016**, *124*, 222–227. [[CrossRef](#)]
15. Nyaba, L.; Matong, J.M.; Nomngongo, P.N. Nanoparticles consisting of magnetite and Al₂O₃ for ligandless ultrasound-assisted dispersive solid phase microextraction of Sb, Mo and V prior to their determination by ICP-OES. *Microchim. Acta* **2016**, *183*, 1289–1297. [[CrossRef](#)]
16. Ondrasek, G.; Rengel, Z.; Romic, D. Humic acids decrease uptake and distribution of trace metals, but not the growth of radish exposed to cadmium toxicity. *Ecotoxicol. Environ. Saf.* **2018**, *151*, 55–61. [[CrossRef](#)] [[PubMed](#)]

17. Biata, N.R.; Mashile, G.P.; Ramontja, J.; Mketi, N.; Nomngongo, P.N. Application of ultrasound-assisted cloud point extraction for preconcentration of antimony, tin and thallium in food and water samples prior to ICP-OES determination. *J. Food Compos. Anal.* **2019**, *76*, 14–21. [[CrossRef](#)]
18. Chen, S.; Zhu, S.; Lu, D. Dispersive micro-solid phase extraction combined with dispersive liquid-liquid microextraction for speciation analysis of antimony by electrothermal vaporization inductively coupled plasma mass spectrometry. *Spectrochim. Acta Part B At. Spectrosc.* **2018**, *139*, 70–74. [[CrossRef](#)]
19. Zhang, D.; Zhao, Y.; Xu, H.-B. Sb (III)-imprinted organic-inorganic hybrid sorbent prepared by hydrothermal-assisted surface imprinting technique for selective adsorption of Sb (III). *Russ. J. Phys. Chem. A* **2018**, *92*, 575–581. [[CrossRef](#)]
20. Xie, C.; Huang, X.; Wei, S.; Xiao, C.; Cao, J.; Wang, Z. Novel dual-template magnetic ion imprinted polymer for separation and analysis of Cd²⁺ and Pb²⁺ in soil and food. *J. Clean. Prod.* **2020**, *262*, 121387. [[CrossRef](#)]
21. Luo, J.; Luo, X.; Crittenden, J.; Qu, J.; Bai, Y.; Peng, Y.; Li, J. Removal of antimonite (Sb (III)) and antimonate (Sb (V)) from aqueous solution using carbon nanofibers that are decorated with zirconium oxide (ZrO₂). *Environ. Sci. Technol.* **2015**, *49*, 11115–11124. [[CrossRef](#)]
22. Zou, J.-P.; Liu, H.-L.; Luo, J.; Xing, Q.-J.; Du, H.-M.; Jiang, X.-H.; Luo, X.-B.; Luo, S.-L.; Suib, S.L. Three-dimensional reduced graphene oxide coupled with Mn₃O₄ for highly efficient removal of Sb (III) and Sb (V) from water. *ACS Appl. Mater. Interfaces* **2016**, *8*, 18140–18149. [[CrossRef](#)] [[PubMed](#)]
23. Karcioğlu Karakaş, Z.; Boncukcuoğlu, R.; Hakkı Karakaş, İ. Antimony removal from aqueous solutions using magnetic nickel ferrite (NiFe₂O₄) nanoparticles. *Sep. Sci. Technol.* **2019**, *54*, 1141–1158. [[CrossRef](#)]
24. Batlokwa, B.S.; Chimuka, L.; Tshentu, Z.; Cukrowska, E.; Torto, N. An ion-imprinted polymer for the selective extraction of mercury (II) ions in aqueous media. *Water SA* **2012**, *38*, 255–260. [[CrossRef](#)]
25. Wu, S.; Dai, X.; Cheng, T.; Li, S. Highly sensitive and selective ion-imprinted polymers based on one-step electrodeposition of chitosan-graphene nanocomposites for the determination of Cr (VI). *Carbohydr. Polym.* **2018**, *195*, 199–206. [[CrossRef](#)] [[PubMed](#)]
26. Pinheiro, S.C.L.; Descalzo, A.B.; Raimundo, I.M.; Orellana, G.; Moreno-Bondi, M.C. Fluorescent ion-imprinted polymers for selective Cu (II) optosensing. *Anal. Bioanal. Chem.* **2012**, *402*, 3253–3260. [[CrossRef](#)] [[PubMed](#)]
27. Fan, H.-T.; Tang, Q.; Sun, Y.; Zhang, Z.-G.; Li, W.-X. Selective removal of antimony (III) from aqueous solution using antimony (III)-imprinted organic-inorganic hybrid sorbents by combination of surface imprinting technique with sol-Gel process. *Chem. Eng. J.* **2014**, *258*, 146–156. [[CrossRef](#)]
28. Yordanova, T.; Dakova, I.; Balashev, K.; Karadjova, I. Polymeric ion-imprinted nanoparticles for mercury speciation in surface waters. *Microchem. J.* **2014**, *113*, 42–47. [[CrossRef](#)]
29. Kakavandi, M.G.; Behbahani, M.; Omidi, F.; Hesam, G. Application of ultrasonic assisted-dispersive solid phase extraction based on ion-imprinted polymer nanoparticles for preconcentration and trace determination of lead ions in food and water samples. *Food Anal. Methods* **2017**, *10*, 2454–2466. [[CrossRef](#)]
30. Yuan, G.; Tu, H.; Liu, J.; Zhao, C.; Liao, J.; Yang, Y.; Yang, J.; Liu, N. A novel ion-imprinted polymer induced by the glycyglycine modified metal-organic framework for the selective removal of Co (II) from aqueous solutions. *Chem. Eng. J.* **2018**, *333*, 280–288. [[CrossRef](#)]
31. Abdullah; Balouch, A.; Talpur, F.N.; Kumar, A.; Shah, M.T.; Mahar, A.M.; Amina. Synthesis of ultrasonic-assisted lead ion imprinted polymer as a selective sorbent for the removal of Pb²⁺ in a real water sample. *Microchem. J.* **2019**, *146*, 1160–1168.
32. Sadani, M.; Rasolevandi, T.; Azarpira, H.; Mahvi, A.H.; Ghaderpoori, M.; Mohseni, S.M.; Atamaleki, A. Arsenic selective adsorption using a nanomagnetic ion imprinted polymer: Optimization, equilibrium, and regeneration studies. *J. Mol. Liq.* **2020**, *317*, 114246. [[CrossRef](#)]
33. Samandari, L.; Bahrami, A.; Shamsipur, M.; Farzin, L.; Hashemi, B. Electrochemical preconcentration of ultra-trace Cd²⁺ from environmental and biological samples prior to its determination using carbon paste electrode impregnated with ion imprinted polymer nanoparticles. *Int. J. Environ. Anal. Chem.* **2019**, *1*–15. [[CrossRef](#)]
34. Ma, J.; Yan, M.; Feng, G.; Ying, Y.; Chen, G.; Shao, Y.; She, Y.; Wang, M.; Sun, J.; Zheng, L.; et al. An overview on molecular imprinted polymers combined with surface-enhanced Raman spectroscopy chemical sensors toward analytical applications. *Talanta* **2021**, *225*, 122031. [[CrossRef](#)] [[PubMed](#)]
35. Fan, J.; Qiu, L.; Zheng, W.; Meng, Z.; Xue, M.; Qiao, Y. Rapid self-assembly preparation of p-nitrophenol-molecular imprinted photonic crystal sensors. *Microchem. J.* **2021**, *164*, 105950. [[CrossRef](#)]
36. Özcan, N.; Medetalibeyoglu, H.; Akyıldırım, O.; Atar, N.; Yola, M.L. Electrochemical detection of amyloid-β protein by delaminated titanium carbide MXene/multi-walled carbon nanotubes composite with molecularly imprinted polymer. *Mater. Today Commun.* **2020**, *23*, 101097. [[CrossRef](#)]
37. Chen, B.; Xie, Q.; Zhang, S.; Lin, L.; Zhang, Y.; Zhang, L.; Jiang, Y.; Zhao, M. A novel electrochemical molecularly imprinted sensor based on CuCo₂O₄@ biomass derived carbon for sensitive detection of tryptophan. *J. Electroanal. Chem.* **2021**, *901*, 115680. [[CrossRef](#)]
38. Kaya, H.K.; Cinar, S.; Altundal, G.; Bayramlı, Y.; Unaleroglu, C.; Kuralay, F. A novel design thia-bilane structure-based molecular imprinted electrochemical sensor for sensitive and selective dopamine determination. *Sens. Actuators B Chem.* **2021**, *346*, 130425. [[CrossRef](#)]

39. Wang, L.; Luo, Y.; Li, H.; Yu, D.; Wang, Y.; Wang, W.; Wu, M. Preparation and selective adsorption of surface-imprinted microspheres based on hyperbranched polyamide—functionalized sodium alginate for the removal of Sb (III). *Colloids Surf. A Physicochem. Eng. Asp.* **2020**, *585*, 124106. [[CrossRef](#)]
40. Fang, L.; Xiao, X.; Kang, R.; Ren, Z.; Yu, H.; Pavlostathis, S.G.; Luo, J.; Luo, X. Highly selective adsorption of antimonite by novel imprinted polymer with microdomain confinement effect. *J. Chem. Eng. Data* **2018**, *63*, 1513–1523. [[CrossRef](#)]
41. Shakerian, F.; Dadfarnia, S.; Shabani, A.M.H. Synthesis of nano-pore size Al (III)-imprinted polymer for the extraction and preconcentration of aluminum ions. *J. Iran. Chem. Soc.* **2013**, *10*, 669–676. [[CrossRef](#)]
42. Zhang, D.; Zhao, Y.; Xu, H.-B. Hydrothermal-assisted derived ion-imprinted sorbent for preconcentration of antimony (III) in water samples. *Sep. Sci. Technol.* **2017**, *52*, 1938–1945. [[CrossRef](#)]
43. Safa, F.; Alinezhad, Y. Ternary nanocomposite of SiO₂/Fe₃O₄/Multi-Walled Carbon Nanotubes for Efficient Adsorption of Malachite Green: Response Surface Modeling, Equilibrium Isotherms and Kinetics. *Silicon* **2019**, *12*, 1619–1637. [[CrossRef](#)]
44. Shakerian, F.; Dadfarnia, S.; Shabani, A.M.H.; MaryamNili, A. Synthesis and characterisation of nano-pore antimony imprinted polymer and its use in the extraction and determination of antimony in water and fruit juice samples. *Food Chem.* **2014**, *145*, 571–577. [[CrossRef](#)]
45. Muckoya, V.A.; Njobeh, P.B.; Nomngongo, P.N.; Ngila, J.C. Ultrasonic-Assisted Magnetic Solid-Phase Dispersive Extraction for Determination of Chlorpyrifos and Triclosan in Wastewater Samples prior to Liquid Chromatography Tandem Mass Spectrometry Detection. *Chromatographia* **2020**, *83*, 373–383. [[CrossRef](#)]
46. Ahmad, M.; Wang, J.; Xu, J.; Zhang, Q.; Zhang, B. Magnetic tubular carbon nanofibers as efficient Cu (II) ion adsorbent from wastewater. *J. Clean. Prod.* **2020**, *252*, 119825. [[CrossRef](#)]
47. Wang, H.; Lin, Y.; Li, Y.; Dolgoma, A.; Fang, H.; Guo, L.; Huang, J.; Yang, J. A novel magnetic Cd (II) ion-imprinted polymer as a selective sorbent for the removal of cadmium ions from aqueous solution. *J. Inorg. Organomet. Polym. Mater.* **2019**, *29*, 1874–1885. [[CrossRef](#)]
48. Zhou, Z.; Liu, X.; Zhang, M.; Jiao, J.; Zhang, H.; Du, J.; Zhang, B.; Ren, Z. Preparation of highly efficient ion-imprinted polymers with Fe₃O₄ nanoparticles as carrier for removal of Cr (VI) from aqueous solution. *Sci. Total Environ.* **2020**, *699*, 134334. [[CrossRef](#)]
49. Nomngongo, P.N.; Ngila, J.C. Multivariate optimization of dual-bed solid phase extraction for preconcentration of Ag, Al, As and Cr in gasoline prior to inductively coupled plasma optical emission spectrometric determination. *Fuel* **2015**, *139*, 285–291. [[CrossRef](#)]
50. Mitreva, M.; Dakova, I.; Karadjova, I. Iron (II) ion imprinted polymer for Fe (II)/Fe (III) speciation in wine. *Microchem. J.* **2017**, *132*, 238–244. [[CrossRef](#)]
51. Liu, P.; An, H.; Ren, Y.; Feng, J.; Ma, J. Selective recognition mechanism of molybdenum (VI) ions binding onto ion-imprinted particle in the water. *Chem. Eng. J.* **2018**, *349*, 176–183. [[CrossRef](#)]
52. Xie, C.; Wei, S.; Chen, D.; Lan, W.; Yan, Z.; Wang, Z. Preparation of magnetic ion imprinted polymer with waste beer yeast as functional monomer for Cd (II) adsorption and detection. *RSC Adv.* **2019**, *9*, 23474–23483. [[CrossRef](#)]
53. De Oliveira, L.L.G.; Ferreira, G.O.; Suquila, F.A.C.; de Almeida, F.G.; Bertoldo, L.A.; Segatelli, M.G.; Ribeiro, E.S.; Tarley, C.R.T. Development of new analytical method for preconcentration/speciation of inorganic antimony in bottled mineral water using FIA-HG AAS system and SiO₂/Al₂O₃/SnO₂ ternary oxide. *Food Chem.* **2019**, *294*, 405–413. [[CrossRef](#)] [[PubMed](#)]
54. Gürkan, R.; Eser, M. Application of ultrasonic-assisted cloud point extraction/flame atomic absorption spectrometry (UA-CPE/FAAS) for preconcentration and determination of low levels of antimony in some beverage samples. *J. Iran. Chem. Soc.* **2016**, *13*, 1579–1591. [[CrossRef](#)]
55. Karlıdağ, N.E.; Toprak, M.; Tekin, Z.; Bakırdere, S. Zirconium nanoparticles based ligandless dispersive solid phase extraction for the determination of antimony in bergamot and mint tea samples by slotted quartz tube-flame atomic absorption spectrophotometry. *J. Food Compos. Anal.* **2020**, *92*, 103583. [[CrossRef](#)]
56. You, N.; Liu, T.-H.; Fan, H.-T.; Shen, H. An efficient mercapto-functionalized organic—inorganic hybrid sorbent for selective separation and preconcentration of antimony (III) in water samples. *RSC Adv.* **2018**, *8*, 5106–5113. [[CrossRef](#)]
57. Zhang, Y.; Ma, J.; Na, X.; Shao, Y.; Liu, J.; Mao, X.; Chen, G.; Tian, D.; Qian, Y. A portable and filed optical emission spectrometry coupled with microplasma trap for high sensitivity analysis of arsenic and antimony simultaneously. *Talanta* **2020**, *218*, 121161. [[CrossRef](#)] [[PubMed](#)]
58. Zhang, Y.; Mei, M.; Ouyang, T.; Huang, X. Preparation of a new polymeric ionic liquid-based sorbent for stir cake sorptive extraction of trace antimony in environmental water samples. *Talanta* **2016**, *161*, 377–383. [[CrossRef](#)] [[PubMed](#)]
59. Zhu, Z.; Yang, C.; Yu, P.; Zheng, H.; Liu, Z.; Xing, Z.; Hu, S. Determination of antimony in water samples by hydride generation coupled with atmospheric pressure glow discharge atomic emission spectrometry. *J. Anal. At. Spectrom.* **2019**, *34*, 331–337. [[CrossRef](#)]
60. Zmit, B.; Belhaneche-Bensemra, N. Antimony leaching from PET plastic into bottled water in Algerian market. *Environ. Monit. Assess.* **2019**, *191*, 749. [[CrossRef](#)]
61. Khan, M.W.; Khalid, M.; HabibUllah, H.U.R.; Ayaz, Y.; Ullah, F.; Jadoon, M.A.; Afridi, S. Detection of Arsenic (As), Antimony (Sb) and Bacterial Contamination in Drinking Water. *Bio Form.* **2017**, *9*, 133–238.
62. Dos Santos, G.S.; Silva, L.O.B.; Santos, A.F.; da Silva, E.G.P.; Dos Santos, W.N.L. Analytical strategies for determination and environmental impact assessment of inorganic antimony species in natural waters using hydride generation atomic fluorescence spectrometry (HG-AFS). *J. Braz. Chem. Soc.* **2018**, *29*, 185–190. [[CrossRef](#)]

63. Büyükpınar, C.; Bodur, S.; San, N.; Komesli, O.T.; Bakırdere, S. Ultrasonic assisted glass bead loaded gas liquid separator-photochemical vapor generation-T-shaped slotted quartz tube-flame atomic absorption spectrophotometry system for antimony determination in tap water and wastewater samples. *Chem. Pap.* **2021**, *75*, 1377–1386.
64. Du, X.; Qu, F.; Liang, H.; Li, K.; Yu, H.; Bai, L.; Li, G. Removal of antimony (III) from polluted surface water using a hybrid coagulation—flocculation—ultrafiltration (CF—UF) process. *Chem. Eng. J.* **2014**, *254*, 293–301. [[CrossRef](#)]
65. Mitrakas, M.; Mantha, Z.; Tzollas, N.; Stylianou, S.; Katsoyiannis, I.; Zouboulis, A. Removal of Antimony Species, Sb (III)/Sb (V), from Water by Using Iron Coagulants. *Water* **2018**, *10*, 1328. [[CrossRef](#)]
66. Liu, F.; Le, X.C.; McKnight-Whitford, A.; Xia, Y.; Wu, F.; Elswick, E.; Johnson, C.C.; Zhu, C. Antimony speciation and contamination of waters in the Xikuangshan antimony mining and smelting area, China. *Environ. Geochem. Health* **2010**, *32*, 401–413. [[CrossRef](#)]